# Role of spin-3/2 hyperon resonances in the kaon photoproduction $p \to K^+\Lambda$



2017 J. Phys.: Conf. Ser. 856 012011

(http://iopscience.iop.org/1742-6596/856/1/012011)

IOP Conf. Series: Journal of Physics: Conf. Series **856** (2017) 012011 doi:10.1088/1742-6596/856/1/012011

# Role of spin-3/2 hyperon resonances in the kaon photoproduction $\gamma p \to K^+\Lambda$

**W D Suciawo, S Clymton and T Mart**

Departemen Fisika, FMIPA, Universitas Indonesia, Depok 16424, Indonesia

E-mail: samsonclymton@gmail.com

**Abstract.** We have studied the role of spin-3/2 hyperon resonances in the kaon photoproduction $\gamma p \to K^+\Lambda$ by using an isobar model within the effective Lagrangian approach. This study provides an extension to our previous study, which investigated the effect of nucleon resonances with spins up to 5/2. In the current investigation we have added 7 hyperon resonances with spin-3/2 to the model. The result indicates that the inclusion of spin-3/2 hyperon resonances have a significant effect on this model, i.e., the value of $\chi^2$ can be substantially reduced. Significant improvement can be observed in the polarization observables, especially in the backward angles.

## 1. Introduction

It has been a long time since the $\gamma p \to K^+\Lambda$ reaction was used as a tool to investigate the properties of kaon and strangeness degrees of freedom. A number of models have been used in these studies to theoretically explain the process of kaon photoproduction. A notorious problem of the spin-coupling inconsistency showed up, especially in the case of higher spin. It is the purpose of our study to alleviate this problem by using the Pascalutsa [1–3] prescription. The prescription has been used in the previous study [4] to investigate the effect of spin-3/2 and spin-5/2 resonance models in the $\gamma p \to K^+\Lambda$ reaction. Note that the previous studies only focused on the nucleon resonances because those are directly associated with their total energy. In the present study we will explore the role of spin-3/2 hyperon resonances in kaon photoproduction by using an isobar model. Since the values of coupling constants are mostly unknown, in our calculation we have to extract them from experimental data. Our present database consists of the cross section and polarization observables data, in which more than 7,400 data points are available from different measurements.

## 2. The isobar model

The kaon photoproduction reaction investigated in the present study can be formally written as

$$\gamma(k) + p(p) \to K^+(q) + \Lambda(p_\Lambda) \ . \tag{1}$$

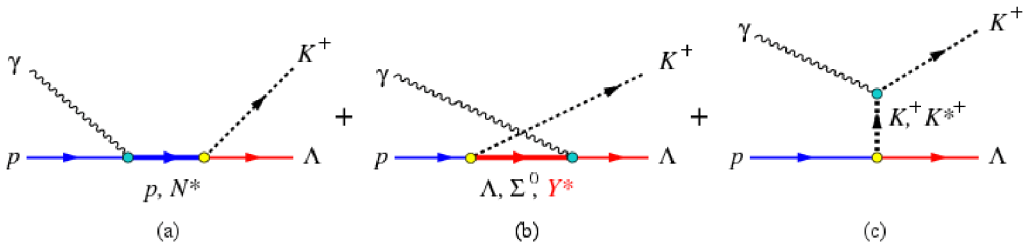


**Figure 1.** Feynmann diagrams for kaon photoproduction $\gamma + p \to K^+ + \Lambda$. Each diagram describes the (a) $s$-channel with proton and nucleon resonance intermediate states, (b) $u$-channel with $\Lambda$, $\Sigma^0$ and hyperon resonance intermediate states and (c) $t$-channel with kaon and kaon resonance intermediate states [5].

The process can be described by means of the $s$-, $u$- and $t$-channel Feynman diagrams depicted in figure 1. The Mandelstam variables are defined as

$$s = (p+k)^2 = W^2 \ , \tag{2}$$
$$t = (k-q)^2 \ , \tag{3}$$
$$u = (k-p_\Lambda)^2 \ . \tag{4}$$

In this study, we derive the scattering amplitude by using the Feynmann diagrams given in figure 1. The relevant channel for calculating the scattering amplitude of hyperon resonance is given in figure 1 (b). The obtained scattering amplitude can be decomposed into (see [4], for instance)

$$\mathcal{M}_{fi} = \bar{u}_\Lambda \sum_{i=1}^{6} A_i(s,t,u,k^2)\, M_i\, u_p \ , \tag{5}$$

where $\bar{u}_\Lambda$ and $u_p$ are $\Lambda$ and proton spinors, respectively. The gauge and Lorentz invariant matrices $M_i$ are given by [6, 7]

$$M_1 = \tfrac{1}{2}\gamma_5(\not\epsilon\not k - \not k\not\epsilon) \ , \tag{6}$$
$$M_2 = \gamma_5\left[(2q-k)\cdot\epsilon\ P\cdot k - (2q\cdot k)\cdot k\ P\cdot\epsilon\right] \ , \tag{7}$$
$$M_3 = \gamma_5(q\cdot k\not\epsilon - q\cdot\epsilon\not k) \ , \tag{8}$$
$$M_4 = i\epsilon_{\mu\nu\rho\sigma}\gamma^\mu q^\nu \epsilon^\rho k^\sigma \ , \tag{9}$$
$$M_5 = \gamma_5(q\cdot\epsilon\ k^2 - q\cdot k\ k\cdot\epsilon) \ , \tag{10}$$
$$M_6 = \gamma_5(k\cdot\epsilon\not k - k^2\not\epsilon) \ , \tag{11}$$

with $P = \frac{1}{2}(p+p_\Lambda)$ and $\epsilon_{\mu\nu\rho\sigma}$ being the four-dimensional Levi-Civita tensor, which is related to the Dirac matrices via $i\epsilon_{\mu\nu\rho\sigma}\gamma^\mu = \gamma_5(-\gamma_\nu\gamma_\rho\gamma_\sigma + g_{\nu\rho}\gamma_\sigma + g_{\rho\sigma}\gamma_\nu - g_{\nu\sigma}\gamma_\rho)$. In the case of photoproduction, we use real photon so that $k\cdot\epsilon = 0 = k^2$. Therefore, both $M_5$ and $M_6$ vanish in the calculation. In the case of electroproduction, the virtual photon has $k^2 \neq 0$. As a consequence, both $M_5$ and $M_6$ may contribute to the scattering amplitude. For the sake of completeness and future studies, in the present study we derive $A_1, \cdots, A_6$. The cross section and other polarization observables can be calculated by means of the functions $A_1, \cdots, A_6$.

To account for the hadronic structure we include hadronic form factors in all hadronic vertices, where we adopt the method developed by Haberzettl [8] to restore the gauge invariance of

amplitudes, which is broken after the inclusion of the form factors. In the present study the hadronic form factor reads

$$F(\Lambda, x) = \frac{\Lambda^4}{\Lambda^4 + (x - m^2)^2} \ , \tag{12}$$

where $\Lambda$ is the form factor cutoff, $m$ is the mass of intermediate particle and $x$ refers to one of the Mandelstam variables. We note that this method introduces two more free parameters, which come from the gauge amplitude $A_2$. Together with the individual form factors, we parameterize this gauge form factor as [8]

$$\tilde{F} \ = \ F(\Lambda, s)\ \sin^2\theta_{\rm had}\ \cos^2\phi_{\rm had} + F(\Lambda, u)\ \sin^2\theta_{\rm had}\ \sin^2\phi_{\rm had} + F(\Lambda, t)\ \cos^2\phi_{\rm had} \ , \tag{13}$$

where the values of $\theta_{\rm had}$ and $\phi_{\rm had}$ are obtained from the fit.

Based on the work of Pascalutsa [2], the propagator for spin-3/2 particle can be written as

$$P^{3/2}_{\mu\nu} = \frac{(\not{p}_\Lambda - \not{k}) + m_{Y^*}}{3(u - m^2_{Y^*} + i\Gamma_{Y^*} m_{Y^*})}\left[\frac{u}{m^2_{Y^*}}(3P_{\mu\nu} + \gamma^\rho\gamma^\sigma P_{\mu\rho}P_{\nu\sigma})\right] \ , \tag{14}$$

where $P_{\mu\nu} = -g_{\mu\nu} + \frac{1}{u}(k - p_\Lambda)_\mu(k - p_\Lambda)_\nu$. We include factor of $u/m^2_{Y^*}$ in (14) in order to regularize the propagator [10, 19]. The hadronic vertex is obtained from [1] and [4], whereas the electromagnetic vertex is taken from our previous works [3, 4].

Therefore the scattering amplitude can be written as

$$\begin{aligned}\mathcal{M}^{\pm}_{fi} \ &= \ \bar{u}_\Lambda\gamma_5\Big[G^1\not{p}_\Lambda(\epsilon^\mu\not{k} - k^\mu\not{\epsilon}) + G^2(k^\mu p_\Lambda\cdot\epsilon - \epsilon^\mu p_\Lambda\cdot k) + G^3 p^\mu_\Lambda(\not{\epsilon}\not{k} - \not{k}\not{\epsilon})\Big] \\ &\quad \times(\not{p}_\Lambda - \not{k} \pm m_{Y^*})(3P_{\mu\nu} + \gamma^\rho\gamma^\sigma P_{\mu\rho}P_{\nu\sigma})\Big[p^\nu(\not{k} - \not{p}_\Lambda)\Big]u_p \ ,\end{aligned} \tag{15}$$

where

$$G^i = \frac{u\ g_{KY^*p}\ g^i}{3m^6_{Y^*}(u - m^2_{Y^*} + i\Gamma_{Y^*}m_{Y^*})} \ , \tag{16}$$

and

$$g^1 \ = \ -2ig^a_{\gamma\Lambda Y^*} + ig^c_{\gamma\Lambda Y^*} - g^d_{\gamma\Lambda Y^*} \ , \tag{17}$$

$$g^2 \ = \ -2ig^a_{\gamma\Lambda Y^*} - g^b_{\gamma\Lambda Y^*} + 2ig^c_{\gamma\Lambda Y^*} - 2g^d_{\gamma\Lambda Y^*} \ , \tag{18}$$

$$g^3 \ = \ \ ig^a_{\gamma\Lambda Y^*} - ig^c_{\gamma\Lambda Y^*} \ . \tag{19}$$

By decomposing (15) into $M_i$ matrices, we obtain the amplitude $A_i$

$$\begin{aligned}A_1 \ &= \ \Big[\tfrac{1}{2}m_\Lambda(m_p + m_\Lambda)\big\{4c_p + 3u \pm 3m_\Lambda m_{Y^*} \mp m_p m_{Y^*} + m_\Lambda(\pm\tfrac{2}{u}c_p m_{Y^*} + m_p)\big\} \mp 3b_p m_\Lambda m_{Y^*} \\ &\quad -m_\Lambda(b_\Lambda - k^2)(\pm\tfrac{2}{u}c_p m_{Y^*} + m_p) - 2m_\Lambda m_p(u \mp m_p m_{Y^*}) - 2m_\Lambda c_p(m_p \mp m_{Y^*})\Big]G^1 \\ &\quad +\Big[\tfrac{1}{2}(m_p + m_\Lambda)\big\{ \pm 3m_{Y^*}(b_p - b_\Lambda) - k^2(\pm\tfrac{2}{u}c_p m_{Y^*} + m_p) + m_p(u \mp m_\Lambda m_{Y^*}) \\ &\quad +c_p(m_\Lambda \mp m_{Y^*})\big\} + b_\Lambda(\pm m_p m_{Y^*} - c_p)\Big]G^2 + \Big[6(b_p - c_p)(u \pm m_p m_{Y^*}) - 2c_\Lambda(4c_p \\ &\quad \pm\tfrac{2}{u}c_p m_p m_{Y^*} \mp m_p m_{Y^*} + m_p^2) - 4b_\Lambda(\pm m_p m_{Y^*} - c_p) + 2m_\Lambda\{m_p(u \mp m_p m_{Y^*}) \\ &\quad +c_p(m_p \mp m_{Y^*})\} - 2(m_p + m_\Lambda)\{m_p(u \mp m_\Lambda m_{Y^*}) + c_p(m_\Lambda \mp m_{Y^*})\}\Big]G^3 \ ,\end{aligned} \tag{20}$$

$$\begin{aligned}A_2 \ &= \ \frac{1}{t - m^2_K}\Big[\big\{ \mp 6m_\Lambda m_{Y^*}(b_\Lambda - b_p) - m_\Lambda k^2(m_p \pm \tfrac{2}{u}c_p m_{Y^*} \mp 3m_{Y^*})\big\}G^1 + \big\{k^2\{m_\Lambda(m_p \\ &\quad \pm\tfrac{2}{u}c_p m_{Y^*}) - 3c_p\} - 3(b_\Lambda - b_p)(u \mp m_\Lambda m_{Y^*})\big\}G^2 + \big\{4k^2(\pm m_p m_{Y^*} - c_p)\big\}G^3\Big] \ ,\end{aligned} \tag{21}$$

$$
\begin{aligned}
A_3 &= \Big[\tfrac{1}{2}m_\Lambda\big\{3u \pm 3m_\Lambda m_{Y^*} \mp 3m_p m_{Y^*} - m_\Lambda(\pm\tfrac{2}{u}c_p m_{Y^*} + m_p)\big\}\Big]G^1 + \Big[\tfrac{1}{2}\big\{ \mp 3m_{Y^*}(b_p \\
&\quad +b_\Lambda) + k^2(\pm\tfrac{2}{u}c_p m_{Y^*} + m_p) - m_p(u \mp m_\Lambda m_{Y^*}) - c_p(m_\Lambda \mp m_{Y^*})\big\}\Big]G^2 \\
&\quad +\Big[ \mp 6m_{Y^*}(b_p - c_p) - 2(\pm c_p m_{Y^*} - u m_p) + 2c_\Lambda(\pm\tfrac{2}{u}c_p m_{Y^*} + m_p)\Big]G^3 \ , \qquad (22)\\
A_4 &= \Big[\tfrac{1}{2}m_\Lambda\big\{3u \pm 3m_\Lambda m_{Y^*} \pm 3m_p m_{Y^*} + m_\Lambda(\pm\tfrac{2}{u}c_p m_{Y^*} + m_p)\big\}\Big]G^1 + \Big[\tfrac{1}{2}\big\{ \pm 3m_{Y^*}(b_p \\
&\quad -b_\Lambda) - k^2(\pm\tfrac{2}{u}c_p m_{Y^*} + m_p) + m_p(u \mp m_\Lambda m_{Y^*}) + c_p(m_\Lambda \mp m_{Y^*})\big\}\Big]G^2 \\
&\quad +\Big[ \pm 6m_{Y^*}(b_p - c_p) + 2(\pm c_p m_{Y^*} - u m_p) - 2c_\Lambda(\pm\tfrac{2}{u}c_p m_{Y^*} + m_p)\Big]G^3 \ , \qquad (23)\\
A_5 &= \frac{1}{t - m_K^2}\Big[\big\{ \mp 3m_\Lambda m_{Y^*}(\tfrac{1}{2}k^2 + b_p - b_\Lambda) - m_\Lambda(\pm\tfrac{2}{u}c_p m_{Y^*} + m_p)(\tfrac{3}{2}k^2 - 2b_\Lambda)\big\}G^1 \\
&\quad +\big\{\tfrac{3}{2}(b_p + b_\Lambda)(u \mp m_\Lambda m_{Y^*}) - (2b_\Lambda + \tfrac{1}{2}k^2)\{m_\Lambda(\pm\tfrac{2}{u}c_p m_{Y^*} + m_p) - 3c_p\}\big\}G^2 \\
&\quad -\big\{4(2b_\Lambda + \tfrac{1}{2}k^2)(\pm m_p m_{Y^*} - c_p)\big\}G^3\Big] \ , \qquad (24)\\
A_6 &= \Big[\tfrac{1}{2}m_\Lambda\big\{3(u \pm m_\Lambda m_{Y^*}) + 4c_p \mp m_p m_{Y^*} + m_\Lambda(\pm\tfrac{2}{u}c_p m_{Y^*} + m_p)\big\}\Big]G^1 + \Big[ \mp \tfrac{3}{2}m_{Y^*} \\
&\quad \times(b_p + b_\Lambda) - (b_\Lambda - \tfrac{1}{2}k^2)(\pm\tfrac{2}{u}c_p m_{Y^*} + m_p) - \tfrac{1}{2}m_p(u \mp m_\Lambda m_{Y^*}) \\
&\quad -\tfrac{1}{2}c_p(m_\Lambda \mp m_{Y^*})\Big]G^2 + \Big[2\{m_p(u \mp m_\Lambda m_{Y^*}) + c_p(m_\Lambda \mp m_{Y^*})\}\Big]G^3 \ , \qquad (25)
\end{aligned}
$$

using some notation

$$
\begin{aligned}
b_p &= p \cdot k = \tfrac{1}{2}(s - k^2 - m_p^2) \ , \\
b_\Lambda &= p_\Lambda \cdot k = \tfrac{1}{2}(k^2 + m_\Lambda^2 - u) \ , \\
c_p &= (k - p_\Lambda) \cdot p \ , \\
c_\Lambda &= (k - p_\Lambda) \cdot p_\Lambda \ .
\end{aligned}
$$

to simplify the result of calculation.

The background terms consist of the standard $s$-,$u$- and $t$-channel Born terms including two vector mesons $K^{*+}(892)$ and $K_1(1270)$ [4, 5, 9, 11–17]. Two spin-1/2 hyperon resonances are also included in the model because they have been shown to be important to maintain a reasonable value of the hadronic form-factor cutoff of the Born terms [5]. Meanwhile, all nucleon resonances with spins up to 5/2 listed in the Review of Particle Properties of Particle Data Group (PDG) [18], with at least ** rating, are also included as in our previous study [4]. In the present study, we include all spin-3/2 of $\Lambda$ and $\Sigma$ resonances listed by the PDG [18] with more than ** rating, as can be seen in table 1. This * rating represents evidence of existence of the particle, where **** means evidence of existence is certain and has been proven and explored by many experiments, while * means evidence of existence is poor. In this study, we consider particle with rating at least **, hence quite fair evidence of existence to be included in our calculation.

## 3. Results and discussion

The result of fitting the calculated observables to experimental data is summarized in table 2, where we compare the numerical results of the background properties obtained in the present work with those of the previous study [4].

Obviously, the inclusion of the spin-3/2 hyperon resonances significantly decreases the value of $\chi^2/N$ :

$$
\frac{\chi^2}{N} = \frac{1}{N_{data} - N_{param}} \sum_{i=1}^{N_{data}} \left[\frac{\sigma_i(exp.) - \sigma_i(calc.)}{\delta\sigma_i}\right]^2 \qquad (26)
$$

**Table 1.** List of the hyperon resonances with spin 3/2 included in this study. This table shows the spin, parity, status, mass and width of the hyperon resonances. Entries are taken from the Review of Particle Properties of PDG [18]. $J^P$ represents spin-parity of the particle, and Status represents evidence of existence of the particle, where more stars mean their existence is more certain.

| Particle | $J^P$ | Status | Mass (MeV) | Width (MeV) |
|---|---|---|---|---|
| $\Lambda(1520)$ | $3/2^-$ | **** | $1519.5 \pm 1.0$ | $15.6 \pm 1.0$ |
| $\Lambda(1690)$ | $3/2^-$ | **** | $1690 \pm 5$ | $60 \pm 10$ |
| $\Lambda(1890)$ | $3/2^+$ | **** | $1890^{+10}_{-40}$ | $100^{+100}_{-40}$ |
| $\Sigma(1385)$ | $3/2^+$ | **** | $1383.7 \pm 1.0$ | $36 \pm 5$ |
| $\Sigma(1670)$ | $3/2^-$ | **** | $1670^{+15}_{-5}$ | $60 \pm 20$ |
| $\Sigma(1940)$ | $3/2^-$ | *** | $1940^{+10}_{-40}$ | $220^{+80}_{-70}$ |
| $\Sigma(2080)$ | $3/2^+$ | ** | $2080 \pm 104$ | $186 \pm 48$ |

where $N$ is number of degree of freedom, $N_{data}$ is number of experimental data, $N_{param}$ is number of free parameters that we will fit with experimental data, $\sigma_i(exp.)$ is the $i$-th observable value from expriments, $\sigma_i(calc.)$ is $i$-th observable value from our calculation using isobar model, and $\delta\sigma_i$ is the $i$-th relative error of experimental data. Therefore, the smaller the value of $\chi^2/N$, the better our calculation fitting experimental results.

Figure 2 compares the calculated total cross section obtained in this work and those of the previous studies with various experimental data obtained from different experiments. Clearly, the inclusion of spin-3/2 hyperon resonances in our calculation improves the agreement between the calculated total cross section and the experimental ones, especially around the first peak as well as at higher energies ($\geq 2.25$ GeV).

**Table 2.** The background coupling constants and hadronic cutoff obtained in our previous study [4] (without spin-3/2 hyperon resonances) and those obtained in the present study (with spin-3/2 hyperon resonances). Notation of the parameters is as in our previous study [4].

| Parameters | without [4] | with |
|---|---|---|
| $G_{K\Lambda N}/\sqrt{4\pi}$ | $-3.00$ | $-3.87$ |
| $G_{K\Sigma N}/\sqrt{4\pi}$ | 1.27 | 1.30 |
| $G^V_{K^*}/4\pi$ | 0.15 | $-0.11$ |
| $G^T_{K^*}/4\pi$ | 0.26 | 0.26 |
| $G^V_{K_1}/4\pi$ | 1.46 | $-0.42$ |
| $G^T_{K_1}/4\pi$ | 0.07 | $-0.61$ |
| $G_{\Lambda(1600)}/4\pi$ | 8.41 | $-10.0$ |
| $G_{\Lambda(1810)}/4\pi$ | $-9.61$ | 3.04 |
| $\Lambda_B$(GeV) | 0.70 | 0.94 |
| $\Lambda_R$(GeV) | 1.31 | 1.35 |
| $\theta_{\rm had}$(deg) | 130 | 90.0 |
| $\phi_{\rm had}$(deg) | 177 | 39.7 |
| $\chi^2/N$ | 1.58 | 1.17 |

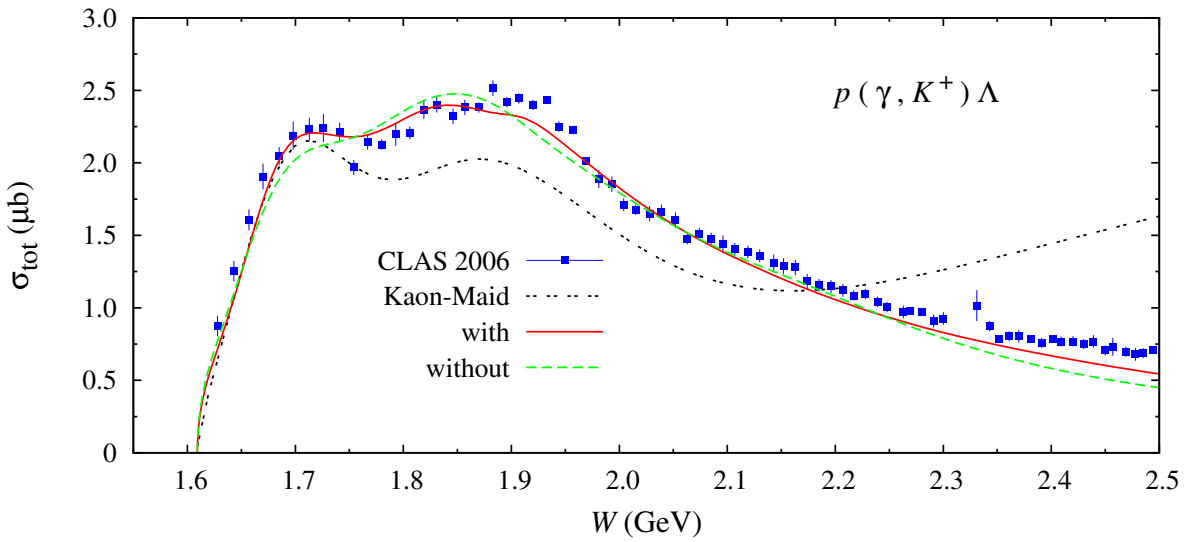


**Figure 2.** Total cross sections obtained in the present study, which includes the spin-3/2 hyperon resonances (solid red line), compared with the calculation without the spin-3/2 hyperon resonances (previous study, dashed green line) [4] and the prediction of Kaon-Maid (dotted black line) [9]. Experimental data (solid blue square) are taken from the CLAS Collaboration [20].

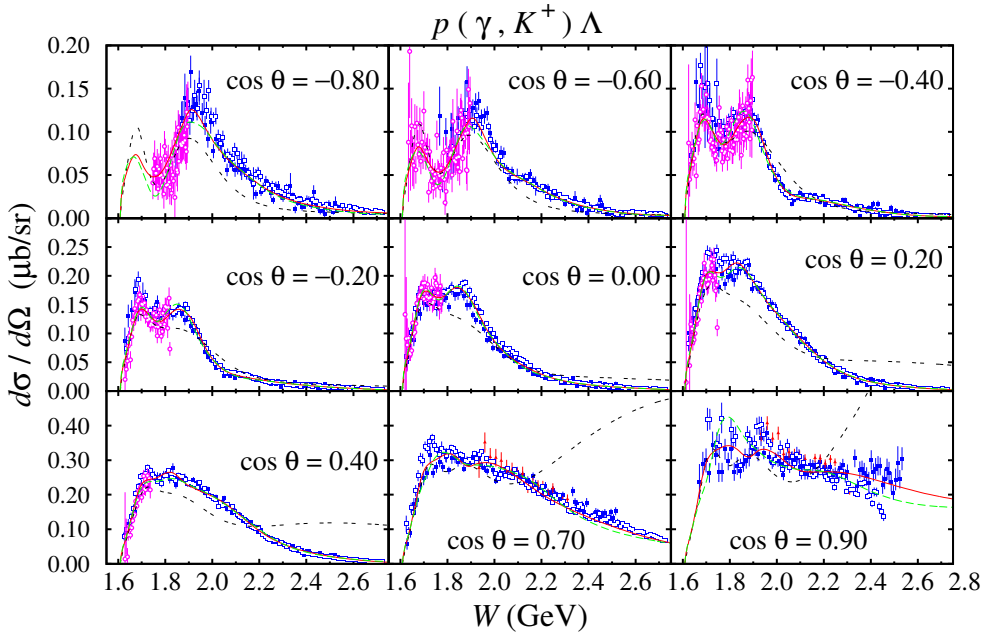


**Figure 3.** Energy distributions of differential cross section for different values of kaon scattering angle. Experimental data are obtained from the CLAS Collaboration (solid squares and open squares) [20, 21], Crystal Ball Collaboration (open circles) [23] and LEPS Collaboration (solid triangles) [22]. Notation of the curves is as in figure 2.

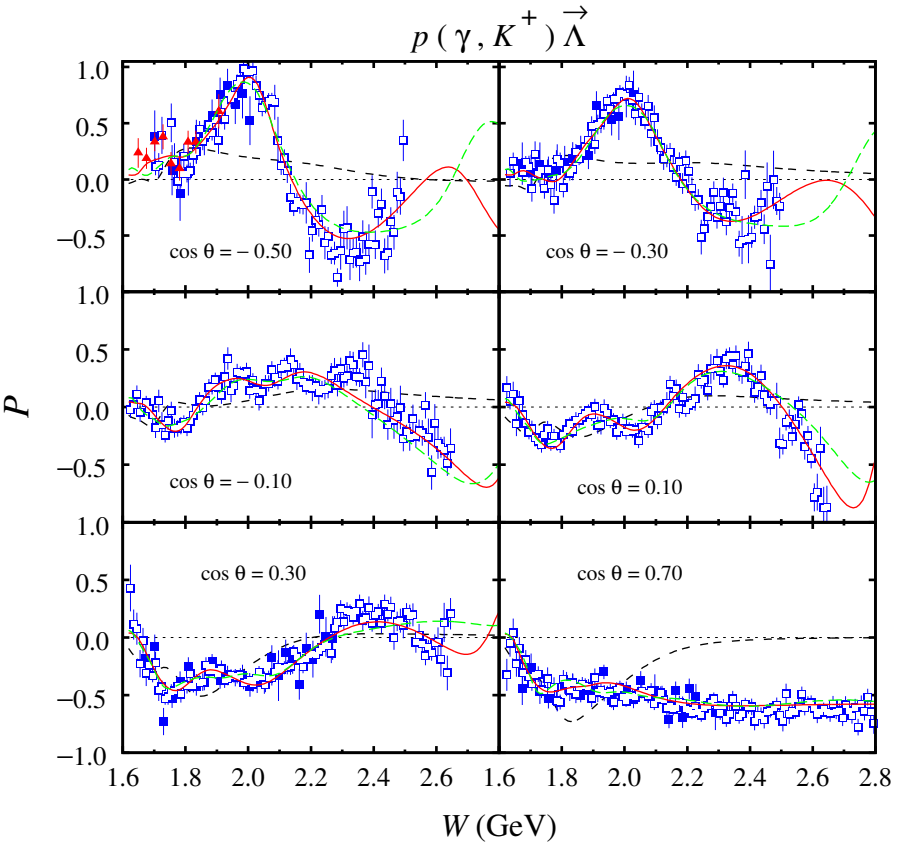


**Figure 4.** Energy distributions of Λ recoil polarization for different values of kaon scattering angle. Experimental data are from the CLAS Collaboration (solid squares and open squares) [20, 21] and the GRAAL Collaboration (solid triangle) [24]. Notation of the curves is as in figure 3.

Figure 3 shows the energy distributions of differential cross section for different values of kaon scattering angles, where we compare experimental data with the calculated differential cross sections obtained from our previous study [4], Kaon-Maid [9] and present investigation. From figure 3 we can conclude that the inclusion of spin-3/2 hyperon resonances has a strong impact at the backward and forward angles. This is understandable since the corresponding Mandelstam variable in the hyperon propagator is $u$, which depends on $\cos\theta$. At $\cos\theta = -0.80$ the inclusion of hyperon resonances can substantially improve the agreement with experimental data around the second peak of the cross section. A similar phenomenon also happens at $\cos\theta = 0.90$, where the improvement seems to be also significant.

Polarization observable has been long known as a decisive constraint for phenomenological models. In the case of kaon photoproduction, the well known and very often used polarization observable is the Λ recoil polarization. The result of our calculation together with those of previous studies are shown in figure 4. In this figure, we can also see that the inclusion of spin-3/2 hyperon resonances provides the best strategy to improve our previous study. Especially at higher energies, the agreement with experimental data is significantly improved. Even though the experimental data is quite scattered in higher energy, this result is able to determine those data better than our previous study.

## 4. Summary and conclusion

We have studied kaon photoproduction by using an isobar model with spin-3/2 hyperon resonances included. This inclusion has been shown to decrease the value of $\chi^2$ significantly. By looking at the polarization observable, we conclude that the spin-3/2 hyperon resonances play an important role especially at the backward angles of kaon photoproduction.

## Acknowledgments

This work has been partly supported by the Research-Cluster-Grant-Program of the University of Indonesia, under contract No. 1862/UN.R12/HKP.05.00/2015.

## References

[1] Pascalutsa V 1998 *Phys. Rev.* D **58** 096002
[2] Pascalutsa V 2001 *Phys. Lett.* B **503** 85
[3] Pascalutsa V and Timmermans R 1999 *Phys. Rev.* C **60** 042201
[4] Mart T, Clymton S and Arifi A J 2015 *Phys. Rev.* D **92** 094019
[5] Mart T and Nurhadiansyah N 2013 *Few-Body Syst.* **54** 1729
[6] Deo B B and Bisoi A K 1974 *Phys. Rev.* D **9** 288
[7] Dennery P 1961 *Phys. Rev.* **124** 2000
[8] Haberzettl H, Bennhold C, Mart T and Feuster T 1998 *Phys. Rev.* C **58** R40
[9] Mart T and Bennhold C 1999 *Phys. Rev.* C **61** 012201
[10] Vrancx T, De Cruz L, Ryckebusch J and Vancraeyveld P 2011 *Phys. Rev.* C **84** 045201
[11] Mart T and Sulaksono A 2006 *Phys. Rev.* C **74** 055203
[12] Mart T 2010 *Phys. Rev.* C **82** 025209
[13] Mart T and Kholili M J 2012 *Phys. Rev.* C **86** 022201
[14] Mart T and Sari A K 2013 *Mod. Phys. Lett.* A **28** 1350054
[15] Mart T 2013 *Phys. Rev.* C **87** 042201
[16] Mart T 2014 *Phys. Rev.* C **90** 065202
[17] Syukurilla L and Mart T 2015 *Int. J. Mod. Phys.* E **24** 1550008
[18] Olive K A *et al* 2014 *Chin. Phys.* C **38** 090001
[19] Shklyar V, Lenske H and Mosel U 2010 *Phys. Rev.* C **82** 015203
[20] Bradford R *et al* 2006 *Phys. Rev.* C **73** 035202
[21] McCracken M E *et al* 2010 *Phys. Rev.* C **81** 025201
[22] Sumihama M *et al* 2006 *Phys. Rev.* C **73** 035214
[23] Jude T C *et al* 2014 *Phys. Lett.* B **735** 112
[24] Lleres A *et al* 2007 *Eur. Phys. J.* A **31** 79
[25] Lleres A *et al* 2009 *Eur. Phys. J.* A **39** 149
[26] Bradford R *et al* 2007 *Phys. Rev.* C **75** 035205